Electronic Supplementary Material (ESI) for Materials Chemistry Frontiers.

Supporting Information

$FeNi_3$ nanoparticles for electrocatalytic synthesis of urea from carbon dioxide and nitrate

Hou et al.

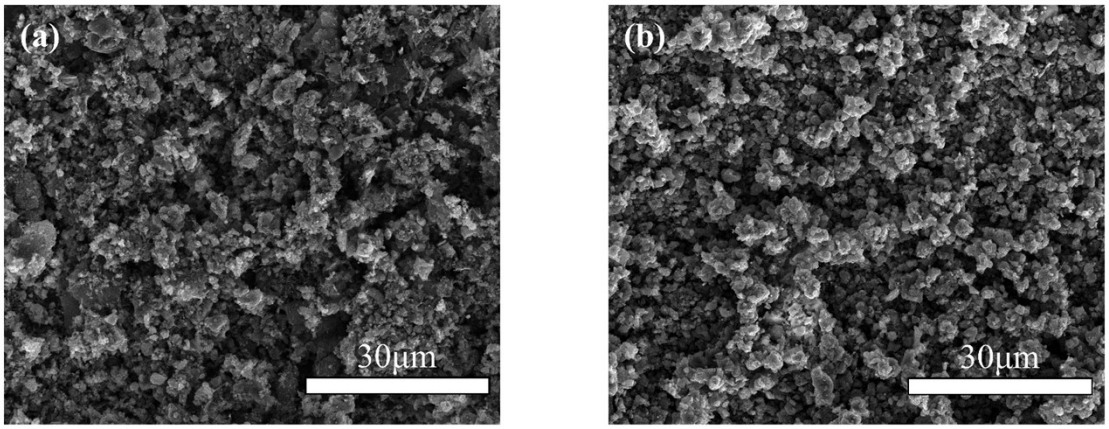

Figure S1. SEM images of (a) Fe/NC and (b) Ni/NC.

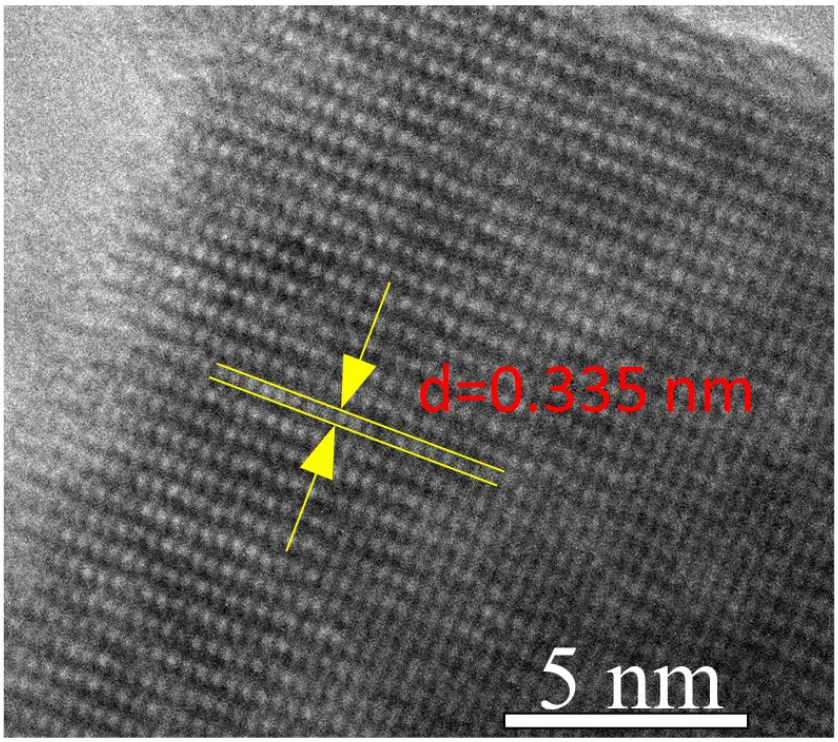

Figure S2. HRTEM images of FeNi/NC.

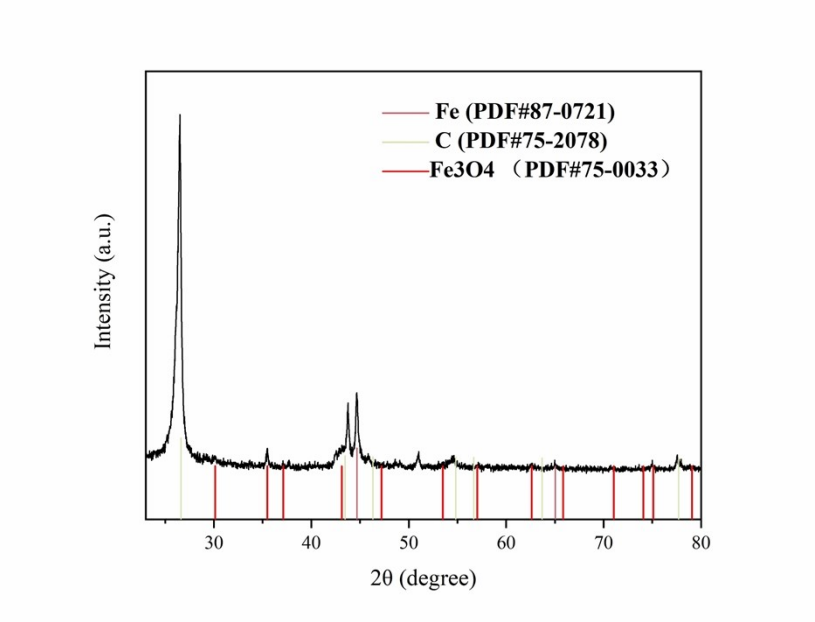

Figure S3. XRD patterns of Fe/NC.

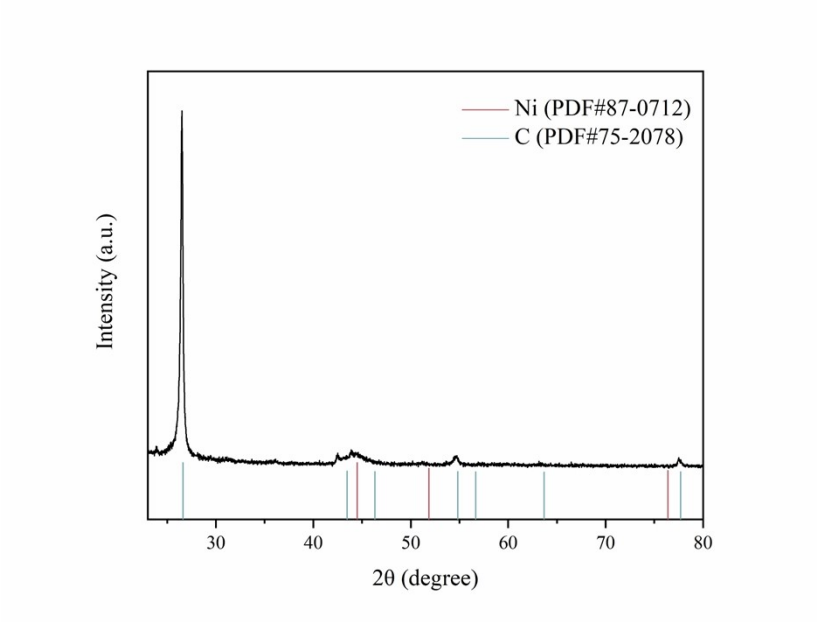

Figure S4. XRD patterns of Ni/NC.

Figure S5. The optical photograph of the H-shaped cell with three-electrode.

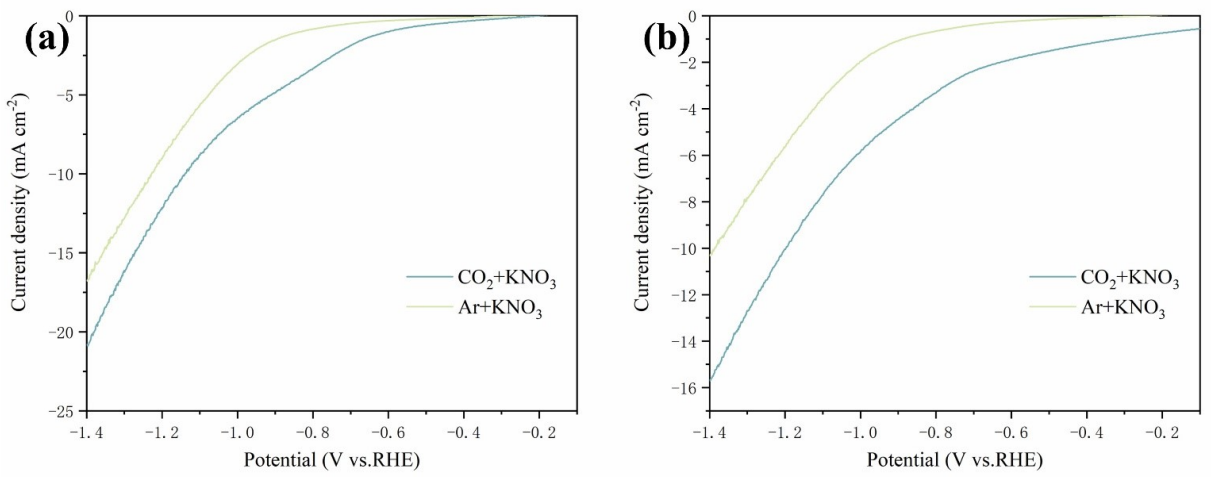

Figure S6. LSV curves for (a) Fe/NC, and (b) Ni/NC in the Ar/CO_2-saturated 0.1 M KNO_3, the scan rate is 10 mV s^{-1}.

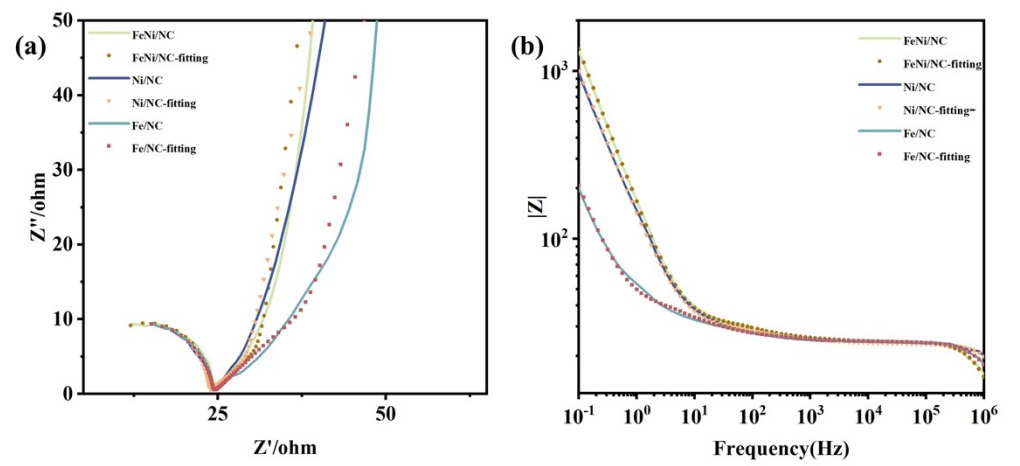

Figure S7. The electrochemical impendence spectra of the FeNi/NC, Fe/NC and NiNC.

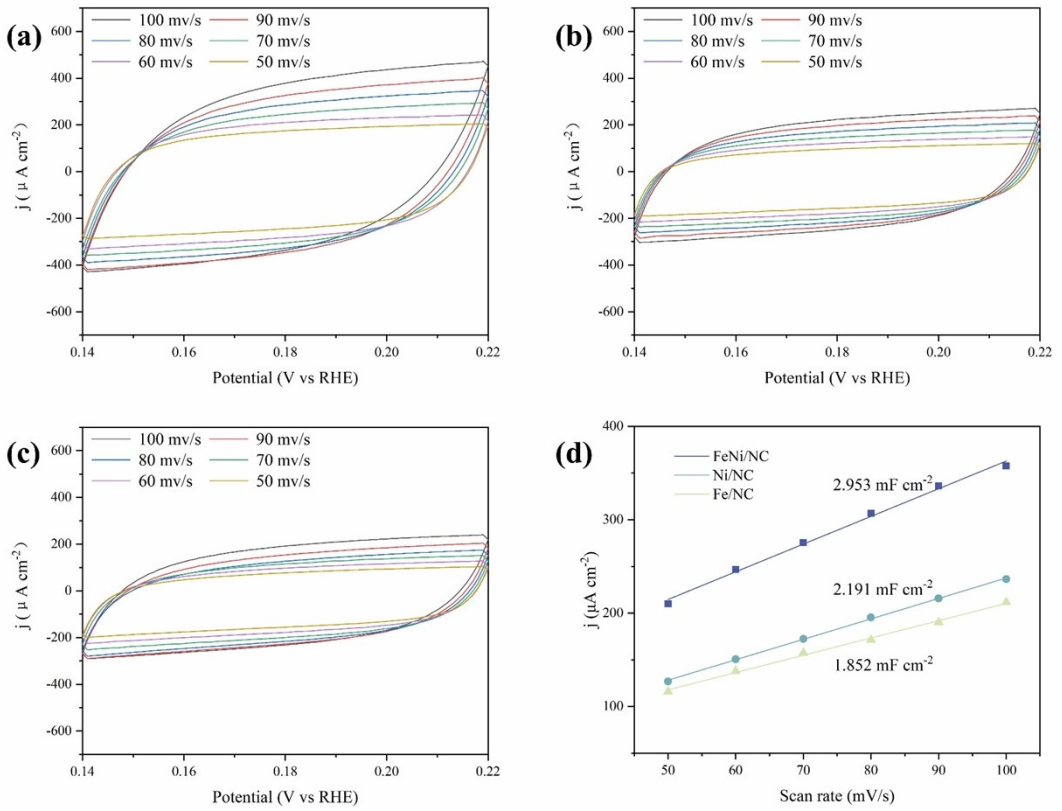

Figure S8. The cyclic voltammograms of (a) FeNi/NC, (b) Ni/NC, and (c) Fe/NC at different scan rates from 50 to 100 mV s^{-1} at the potential window of 0.14 - 0.22 V (vs RHE). (d) The corresponding capacitive current at 0.18 V vs scan rates.

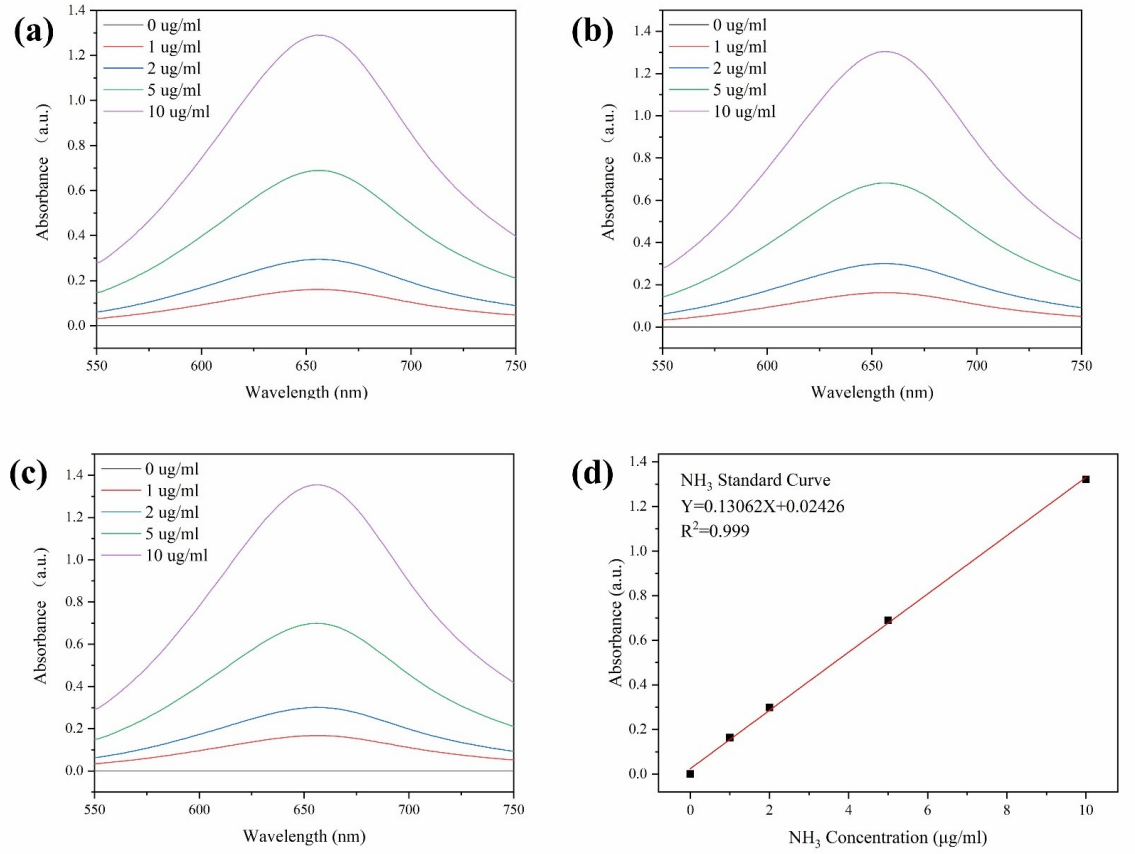

Figure S9. (a-c) UV-vis absorption spectra of various NH_3 concentrations obtained from three repeated experiments. (d) Calibration curve used for estimating NH_3 concentration.

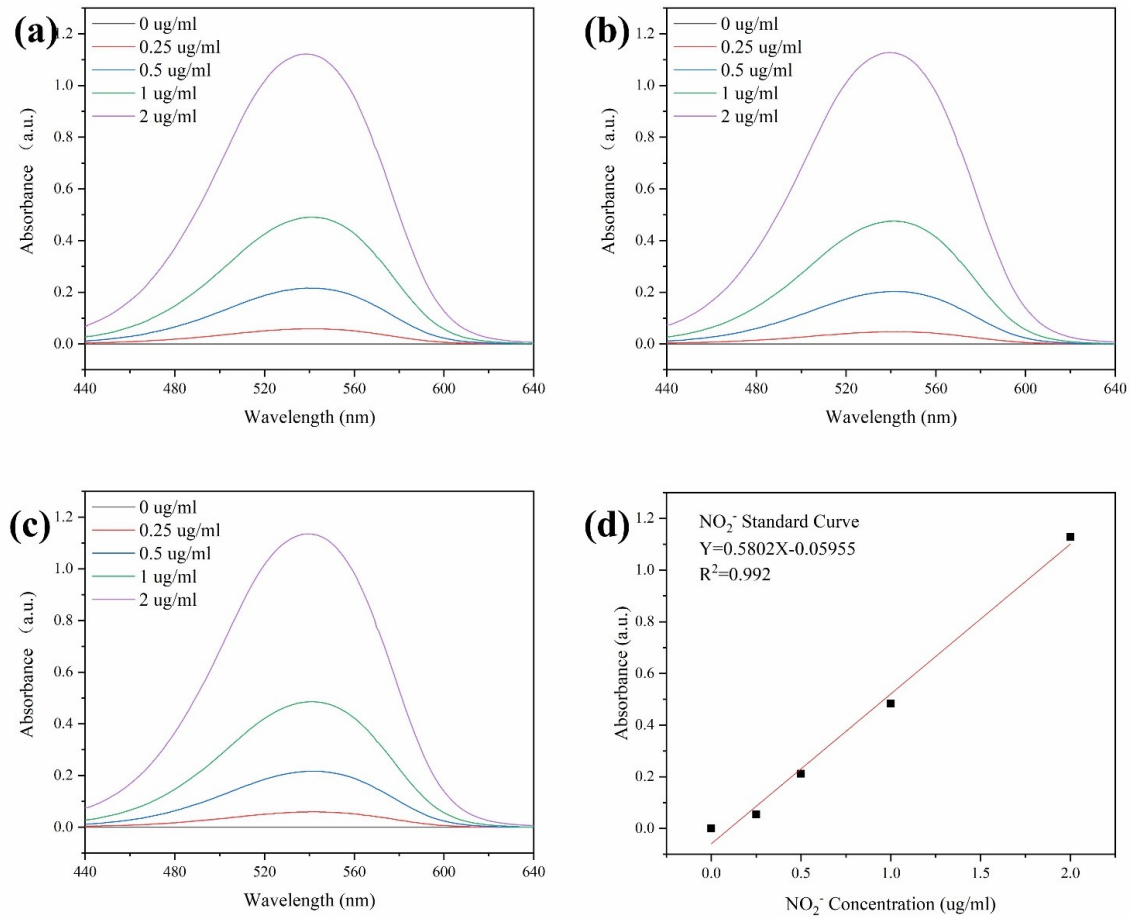

Figure S10. (a-c) UV-Vis absorption spectra of different NO_2^- concentrations obtained from three repeated experiments. (d) Calibration curve used for estimating NO_2^- concentration.

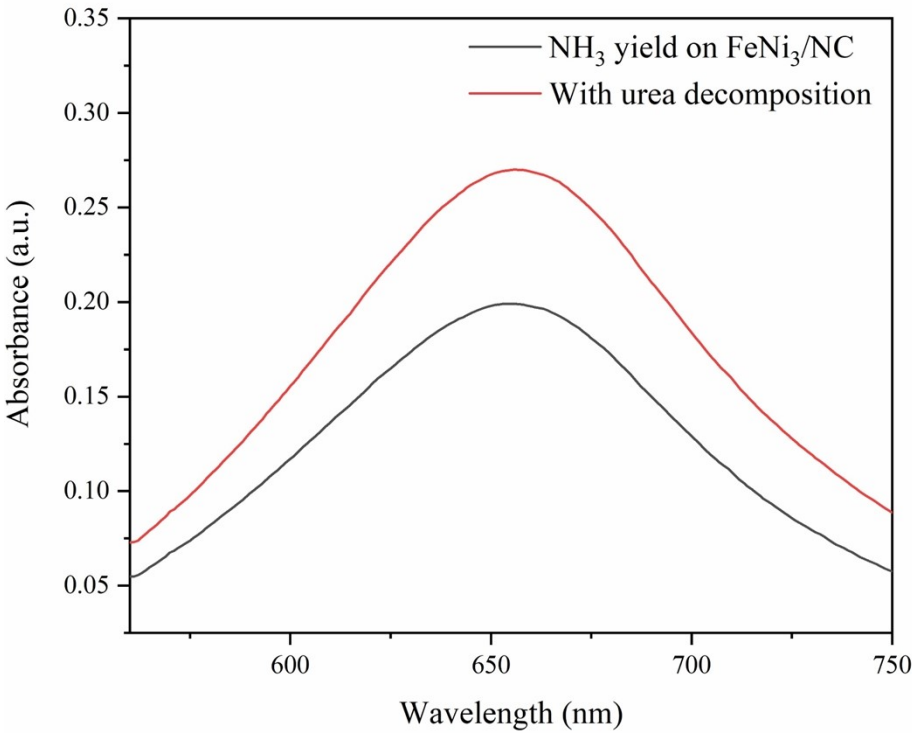

Figure S11. The UV-vis absorbance curve of FeNi/NC under the applied potential of -0.9 V vs RHE with and without urease decomposition.

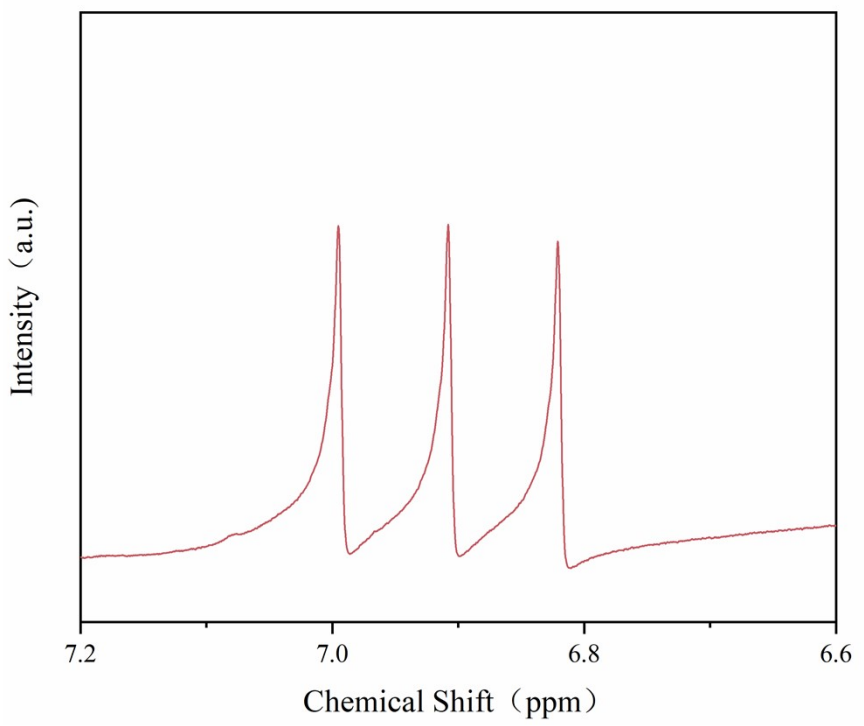

Figure S12. The ^{1}H NMR spectra of identification for electrochemical ammonia synthesis. The ^{1}H NMR spectra of ammonia derived from urea product generation through urease catalysis were obtained from a 0.1 M KNO_3 electrolyte after 1 h of electrolysis of $FeNi_3$/NC catalyst at -0.9 V vs RHE. The electrolyte was then concentrated at 60 °C, resulting in the acquisition of the spectra.

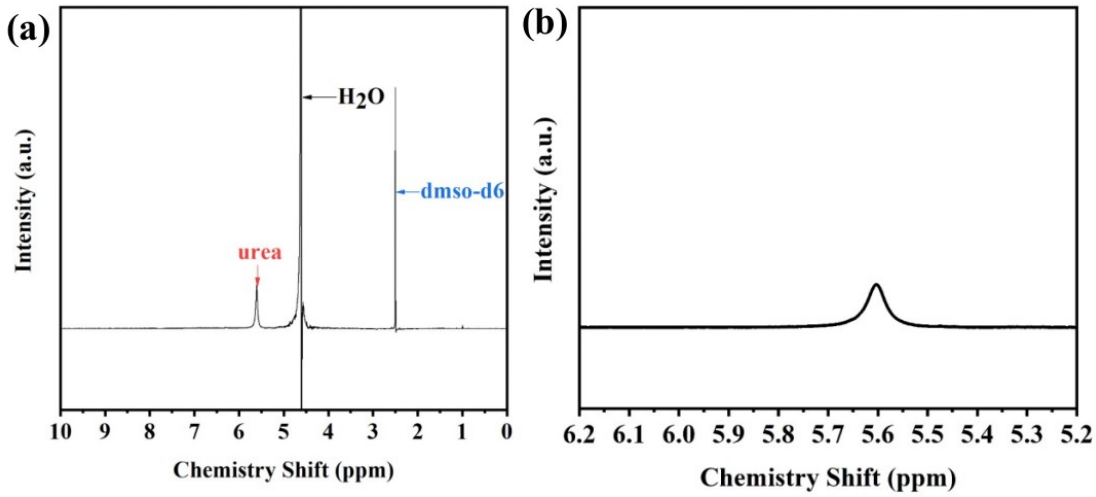

Figure S13. (a) The full ^{1}H NMR spectra. (b) Identification of electrochemical urea synthesis. The ^{1}H NMR spectra of urea were obtained from a 0.1 M KNO_3 electrolyte after 1 h of electrolysis of $FeNi_3$/NC catalyst at -0.9 V vs RHE. The electrolyte was then concentrated at 60 °C, resulting in the acquisition of the spectra.

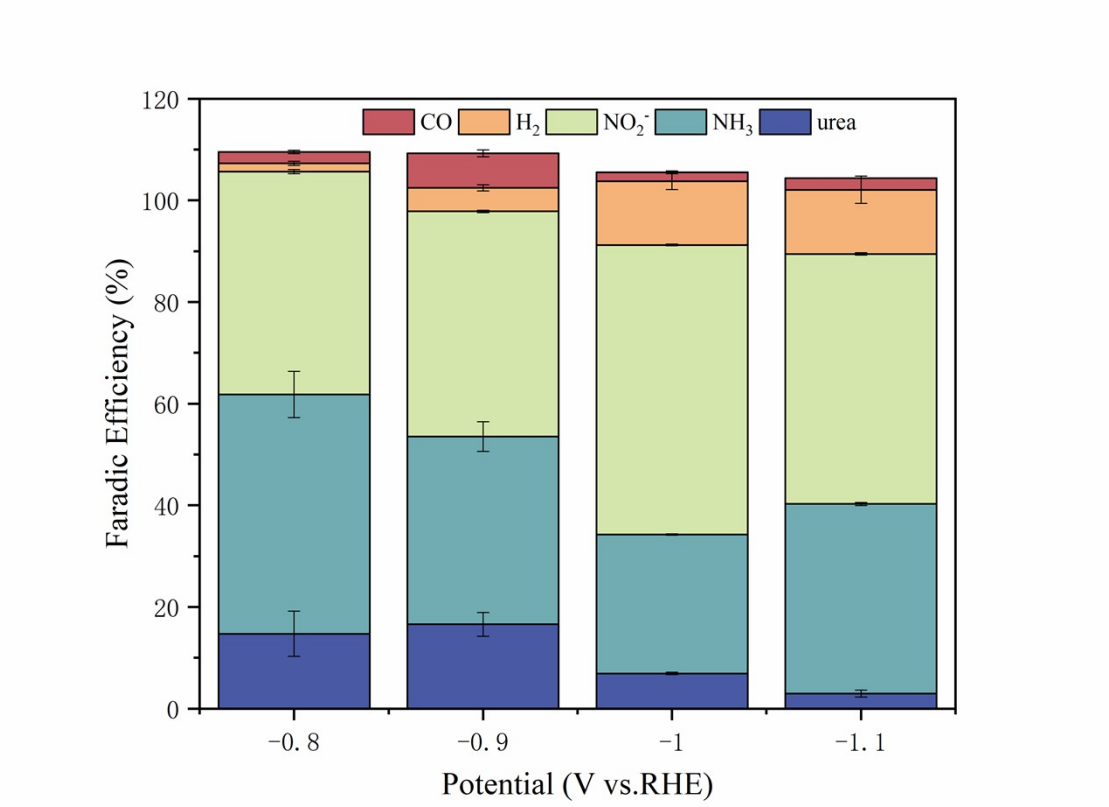

Figure S14. All possible products distribution for FeNi/NC during electrocatalytic urea synthesis at various potentials.

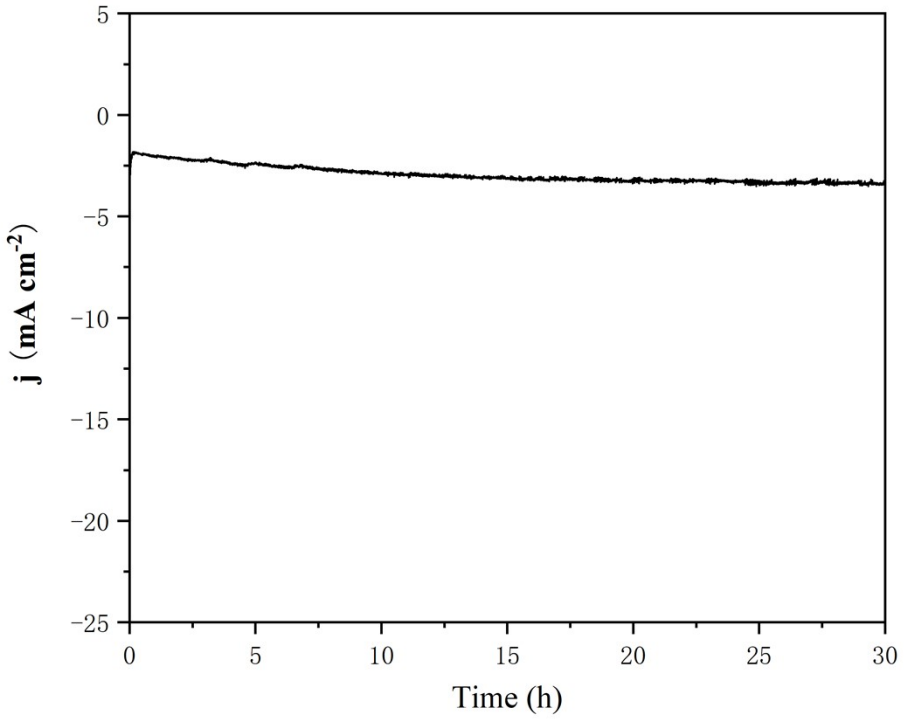

Figure S15. The stability test of the FeNi/ NC at -0.9V vs RHE in CO_2-saturated 0.1 M KNO_3. During the electrochemical synthesis of urea, and no significant decay was observed within 30 h.

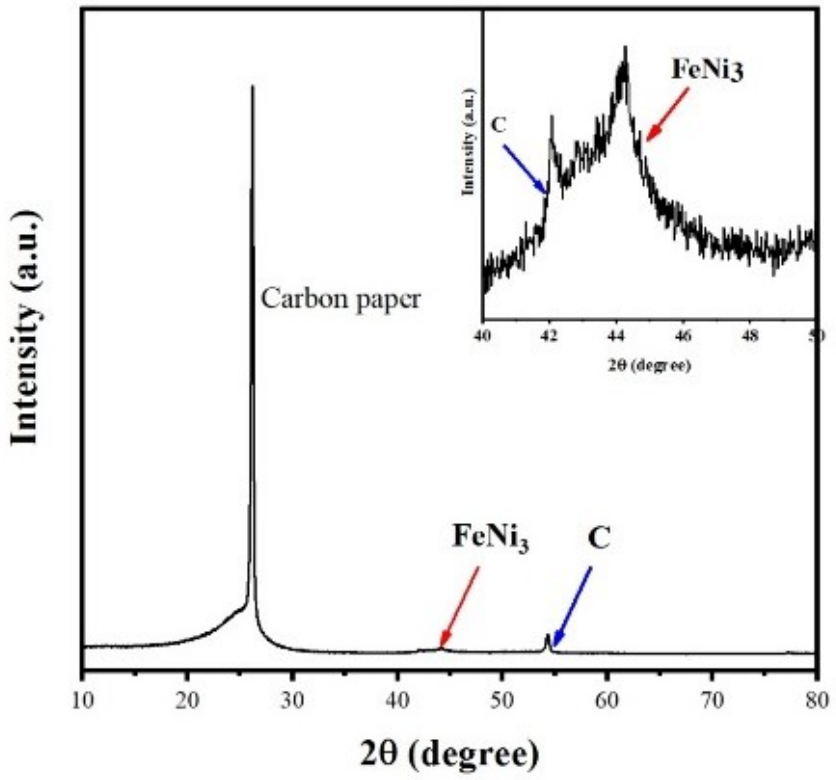

Figure S16. The XRD patterns of FeNi/NC loaded on the carbon paper after 30h stability test.

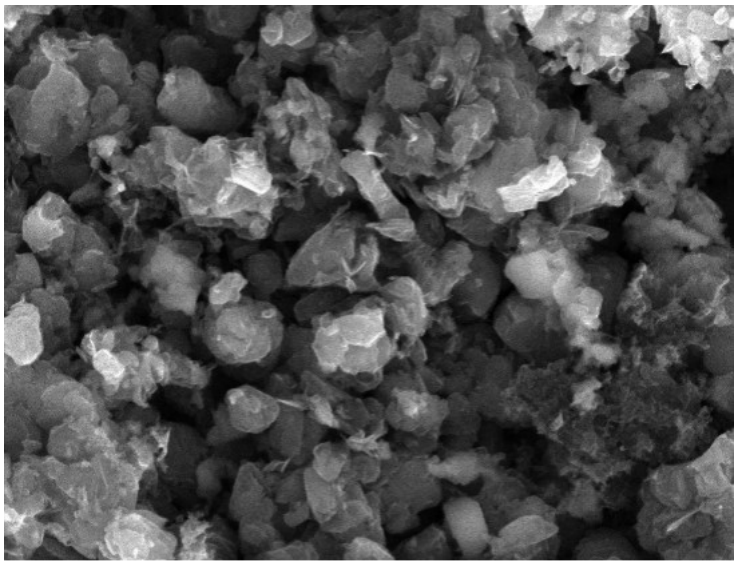

Figure S17. The SEM image of FeNi/NC loaded on the carbon paper after 30 h stability test.

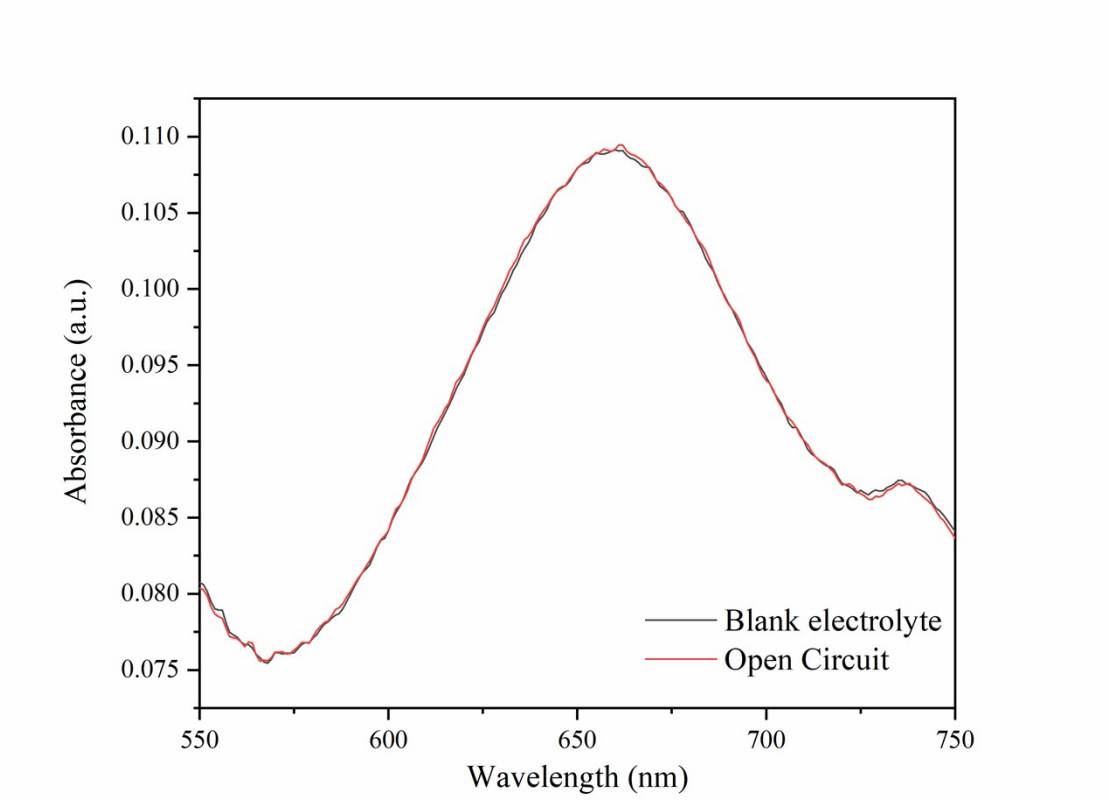

Figure S18. The UV vis absorbance spectra of the blank electrolyte and open circuit opential in CO_2-saturated 0.1 M KNO_3.

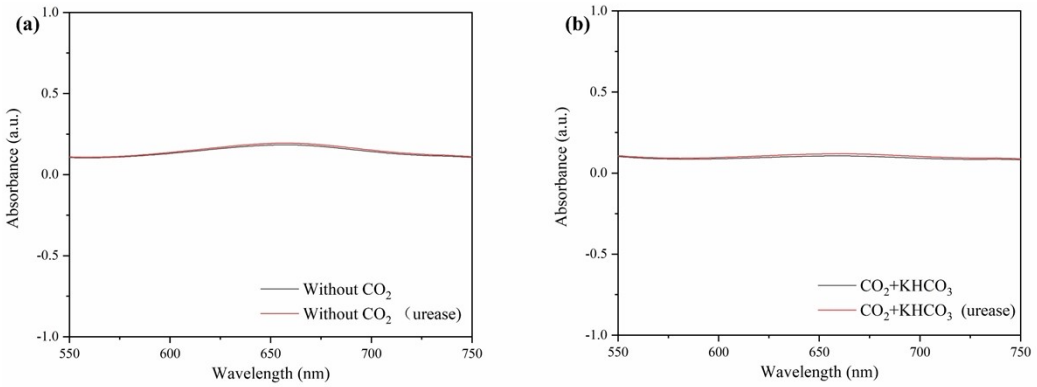

Figure S19. (a) In the absence of CO_2, i.e. CO_2-saturated 0.1 M KNO_3. (b) In the absence of NO_3^-, i.e. CO_2-saturated 0.1 M $KHCO_3$. The absorbance of samples with and without urease was compared, and similar absorbance values were observed in both cases, indicating the absence of urea products.

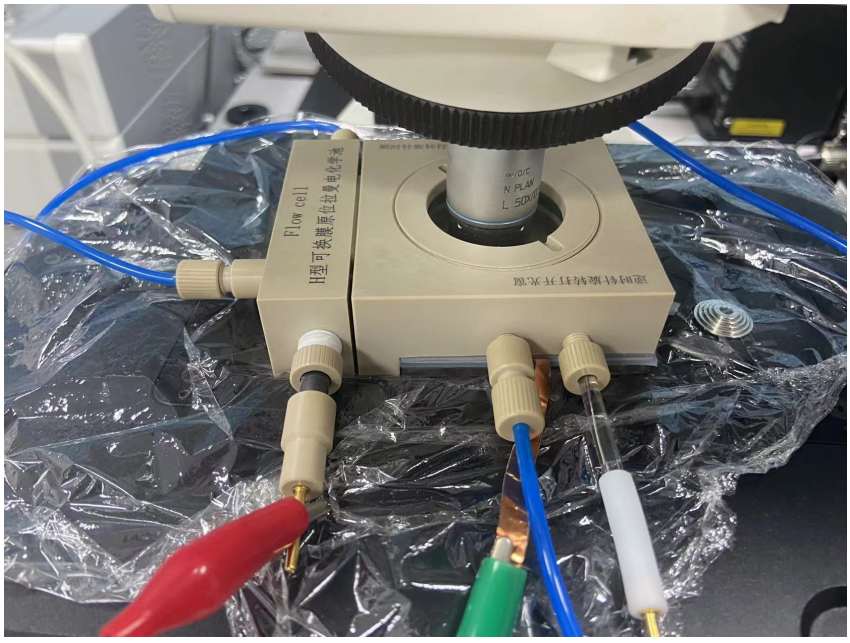

Figure S20. The optical photograph of the in-situ Raman device for urea electrosynthesis analysis.

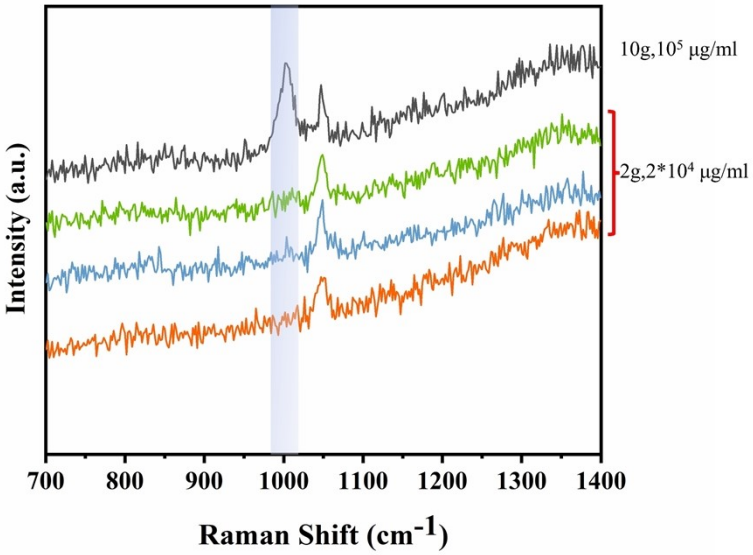

Figure S21. Added 10 g and 2 g of pure urea to the 100 mL 0.1 M KNO_3 electrolyte, resulting in urea concentrations of 10^6 μg/ml and 2×10^5 μg/ml, respectively.

Table S1. Comparison of the electrocatalytic urea production activity of FeNi/NC with previously reported urea electrosynthesis catalysts.

Catalyst	Reactant	Electrolyte	Urea Yield ($\mu g\ h^{-1} mg_{cat}^{-1}$)	FE	Cite
FeNi/NC	NO_3^-+CO_2	0.1 M KNO_3	796.5	16.58%	This work
$In(OH)_3$-S	NO_3^-+CO_2	0.1 M KNO_3	533.1	54.3%	Nat. Sustain. 2021, 4, 868–876.
P_{25}/In/SnO_2	NO_3^-+CO_2	0.1 M KNO_3	NA	40%	Nat. Chem. 2020, 12, 717724.
$Pd_1Cu_1/TiO_2$400	N_2+CO_2	0.1 M $KHCO_3$	201.8	8.9%	Nat. Chem. 2020, 12, 717724.
Bi/BiVO4	N_2+CO_2	0.1 M $KHCO_3$	354.9	12.6%	Angew. Chem. Int. Ed. 2021, 60, 1091010918.
FLPs/InOOH100	N_2+CO_2	0.1 M $KHCO_3$	411.4	20.9%	Chem Catal. 2022, 2(2), 309320.
$BiFeO_3/BiVO_4$	N_2+CO_2	0.1 M $KHCO_3$	296.7	17.2%	Chem Sci. 2021, 12, 6048-6058.
Te–Pd NCs	NO_2^-+CO_2	0.05 M KNO_2	NA	12.2%	Nano Lett. 2020, 20, 8282-8289
Cu-N-C single atoms	NO_3^-+CO_2	0.1 M $KHCO_3$+ 0.1 M KNO_3	1800	28%	Adv. Energy Mater. 2022, 12, 2201500.
F-doped carbon nanotubes	NO_3^-+CO_2	0.1 M KNO_3	381.9	18%	Appl. Catal. B. 2022, 316, 121618

Fe(a)@C/Fe_3O_4-CNTs	NO_3^-+CO_2	0.1 M KNO_3	1341.3±112.6	16.5±6.1%	Angew. Chem. Int. Ed.
V_O-InOOH	NO_3^-+CO_2	0.1 M KNO_3	592.5	51%	ACS Nano 2022, 16 (5), 8213-8222.
ZnO-V	NO_2^-+CO_2	0.2 M $NaHCO_3$+0.1 M $NaNO_2$	5.52mmol·h^{-1}	23.26%	Cell Rep. Phys. Sci. 2021, 2 (3), 100378.
Cu-TiO_2-Vo	NO_2^-+CO_2	0.2 M $HKCO_3$+0.02 M KNO_2	20.8□mol·h^{-1}	43.1%	Nat. Chem. 2020, 12 (8), 717-724.
$Ni_3(BO_3)_2$-150	N_2+CO_2	0.1 M $KHCO_3$	582.6	20.36%	Energy Environ. Sci. 2021, 14 (12), 6605-6615
Vo-CeO_2-750	NO_3^-+CO_2	0.1 M $HKCO_3$+50 mM KNO_3	943.6	NA	J. Am. Chem. Soc.
B-FeNi-DASC	NO_3^-+CO_2	0.1M $KHCO_3$ +50 Mm KNO_3	1213.2	17.8%	Nature Communications 2022,13,5337